Journal of Materials Chemistry A

Accepted Manuscript

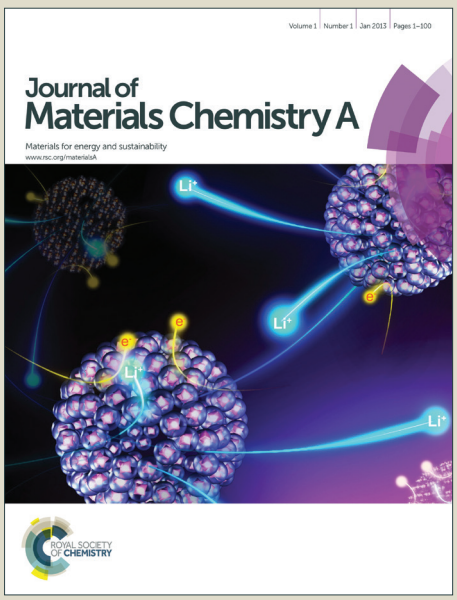

ROYAL SOCIETY OF CHEMISTRY

www.rsc.org/materialsA

Cite this: DOI: 10.1039/c0xx00000x

www.rsc.org/xxxxxx

ARTICLE TYPE

Synthesis of $BiVO_4$ Nanoflake Array Films for Photoelectrochemical Water Oxidation

Huichao He,[a, b] Sean P. Berglund,[a] Alexander J. E. Rettie,[a] William D. Chemelewski,[a] Peng Xiao,[b, c] Yunhuai Zhang,*[b] and C. Buddie Mullins*[a]

Received (in XXX, XXX) Xth XXXXXXXXX 20XX, Accepted Xth XXXXXXXXX 20XX
DOI: 10.1039/b000000x

Because of the potential for application in photoelectrochemical cells for water splitting, synthesis of nanostructured $BiVO_4$ is receiving increasing attention. Here we report a simple new drop-casting method for the first time to synthesize un-doped and doped bismuth vanadate ($BiVO_4$) nanoflake array films. Synthesis parameters such as the amount of polyethylene glycol 600 (PEG-600) and the precursor solution drying time are investigated to optimize the films for photoelectrochemical water oxidation. The $BiVO_4$ films consisting of nanoflakes with an average thickness of 20 nm and length of 2 μm were synthesized from a precursor solution containing Bi^{3+}, V^{3+} and PEG-600 with a Bi: V: PEG-600 volume ratio of 2: 2: 1, dried at 135°C for 55 min. Photoelectrochemical measurements show that the $BiVO_4$ nanoflake array films have higher photoelectrochemical activity than the $BiVO_4$ nanoparticle films. Additionally, the nanoflake arrays were tested after incorporating W and Mo to enhance the photoelectrochemical activity. The 2%W, 6%Mo co-doped $BiVO_4$ nanoflake array films demonstrate the best photoelectrochemical activity with photocurrent densities about 2 times higher than the un-doped $BiVO_4$ nanoflake films and greater than the photocurrents of individually Mo doped or W doped $BiVO_4$ films. The origin of enhanced photoelectrochemical activity for the co-doped film may be due to the improved conductivity through the $BiVO_4$ or slightly enhanced water oxidation kinetics.

1. Introduction

Synthesis of semiconductor nanostructure array films has attracted considerable attention over the past decade, both because of their unique electronic and optical properties, and potential application in photovoltaic or photoelectrochemical devices, such as dye-sensitized solar cells and solar water splitting cells.[1-7] In comparison to bulk semiconductor materials, nanostructure array films can offer direct pathways for carrier transport as well as a large semiconductor-electrolyte interface,[3, 8, 9] which may improve the performance of photoelectrochemical devices such as photoanodes for water oxidation. In recent years, many photoanodes have been synthesized in nanostructured geometries, such as nanotube,[7, 10] nanorod [11, 12] and nanowire [13] arrays. In many instances these nanostructured arrays have shown enhanced efficiency for photoelectrochemical water oxidation.

Monoclinic bismuth vanadate ($BiVO_4$) has been considered a promising material for photoelectrochemical water oxidation due to its moderate bandgap (~2.4 eV) and appropriate band edge

positions,[14, 15] allowing it to absorb as much as 11% of the solar spectrum to drive the water splitting reactions. Assuming a quantum yield of 100% in $BiVO_4$, photocurrents of ~7.5 mA/cm^2 could be achieved under AM1.5 G illumination.[16] However, the best performing films developed to date fall well short of this value. The major limiting factors identified include low mobility of carriers, slow water oxidation kinetics, and high electron-hole recombination rates compared to other semiconductors of interest such as TiO_2 and WO_3.[17-20] To address these issues, several strategies have been developed to improve the photoelectrochemical activity of $BiVO_4$, such as doping with foreign elements (Mo, W),[21-24] hydrogen reduction to create oxygen vacancies,[25] coupling with co-catalysts (FeOOH, Co-Pi)[17, 18, 26, 27] or other semiconductors to form stable heterojunction photoanodes.[28, 29] Another strategy is synthesizing $BiVO_4$ as nanostructured films, in which the photogenerated holes can traverse a shorter distance to be collected at the electrode/solution interface, and thus the holes have a lower chance of recombining with the electrons before participating in electrochemical reactions. Nevertheless, there are only a few reports that describe synthesis of $BiVO_4$ nanostructure array films up to now,[5] and the reported synthetic method relies on relatively complicated procedures and conditions, which implies high cost and low-suitability for implementation on a large scale. We were inspired by work using structure-directing agents with other metal oxides such as ZnO [30] and WO_3[31, 32], to synthesize nanostructured films of $BiVO_4$ using low-cost and scalable techniques.

Herein, we report a new, simple, and cost-effective drop-casting method for synthesizing $BiVO_4$ and Mo and W doped $BiVO_4$ nanoflake array films on fluorine-doped tin oxide (FTO) coated glass substrates. This synthesis technique allows for easy control of both the morphology and chemical composition to improve the photoelectrochemical activity of $BiVO_4$ films. Films ranging in morphology from nanoflake arrays to agglomerated nanoparticles were tested to evaluate their performance as photoanodes. The $BiVO_4$ nanoflake array films showed better photoelectrochemical activity than $BiVO_4$ nanoparticle films. Furthermore, incorporation of 2% W and 6% Mo into the $BiVO_4$ nanoflake array films resulted in higher photoelectrochemical activity compared to the un-doped $BiVO_4$ films.

2. Experimental

2.1 Material Synthesis

$Bi(NO_3)_3{\cdot}xH_2O$ (Alfa Aesar, 99.999%), VCl_3 (Sigma-Aldrich, 97%), $(NH_4)_6Mo_7O_{24}{\cdot}4H_2O$ (Sigma-Aldrich, 99.98%) and $(NH_4)_{10}W_{12}O_{41}{\cdot}5H_2O$ (Sigma-Aldrich, 99.99%) were dissolved separately at a concentration of 75 mM in ethylene glycol (Fischer, 99+%) as metal precursor solutions. 0.85 g polyethylene glycol 600 (PEG-600, Alfa Aesar) was dissolved in 25 mL ethylene glycol to create the structure directing agent solution. The precursor solutions were mixed in the desired Bi: V: W: Mo atomic ratios with PEG-600 solution. Based on the best doping levels from previous work,[22] the Bi: V: W: Mo atomic ratios of the films are as follows: 50: 50: 0: 0 for $BiVO_4$, 48.75: 48.75: 2.5: 0 for 2.5%W doped $BiVO_4$, 47.5: 47.5: 0: 5 for 5%Mo doped $BiVO_4$ and 46: 46: 2: 6 for 2%W, 6% Mo co-doped $BiVO_4$. The typical experimental procedure for synthesizing $BiVO_4$ nanoflake array films in as follows: 500 µL $Bi(NO_3)_3$ solution, 500 µL VCl_3 solution and 250 µL PEG-600 solution were mixed to form a precursor solution that is green color. Next, 200 µL of precursor solution was drop-cast on FTO coated glass substrates (1.5×1.5 cm, Pilkington,TEC15) that had been cleaned and sonicated with enthanol (Fischer, 99+%). The sample was dried in an oven at 135 °C for 55 min and then annealed in air at 500 °C for 2.5

hours, a yellow/orange film was obtained on the FTO substrates. For comparison, different morphologies of $BiVO_4$ films were synthesized via adjusting the synthesis conditions, such as the concentration of PEG-600, and drying time for the precursor solution. All films had the same mass of active material, so that the effects of morphology could be observed.

2.2 Material Characterization

Scanning electron microscopy (SEM) images were acquired using a Zeiss Supra 40 VP SEM. X-ray diffraction (XRD) measurements were taken on a Rigaku Spider X-ray diffractometer using powder samples. X-ray photoelectron spectroscopy (XPS) measurements were performed on a Kratos AXIS Ultra DLD system with monochromated Al-Kα radiation. UV-vis transmission measurements were performed with a Cary 5000 UV-vis spectrometer. For Tauc plots the absorption coefficient (α) was determined by:

$$\alpha = -\ln(10^{-\text{absorbance}})/z \quad (1)$$

where z is the film thickness.

2.3 Electrochemical and Photoelectrochemical Measurements

The electrochemical and photoelectrochemical measurements were conducted using a three-electrode cell, which had a main compartment for the working electrode and two branched compartments separated by fritted disks (Ace Glass, 10-20 μm porosity) for the counter electrode and reference electrode. The working electrode was the as synthesized film which was pressed against an O-ring on the main compartment. It had a backside mask so that the active area was approximately 0.22 cm^2 for both frontside and backside illumination measurements. The counter electrode was a 1 mm diameter Pt wire (99.95%, Alfa Aesar) and the reference electrode was Ag/AgCl (sat. KCl, CH Instruments, CH111). Each compartment of the cell was filled from the same stock of electrolyte solution. The pH of the solution was checked using a bench top pH meter (OAKTON). A CH Instruments 660D electrochemical workstation was employed for the electrochemical measurements.

The illumination source was a 150 W xenon lamp (Newport, Model 9600) with an AM 1.5G filter (Newport). For light measurements the lamp was positioned to provide approximately 100 mW/cm^2 irradiation on the film as measured by a thermopile detector (Newport, Models 1916C and 818-UV). In the present work, the photoelectrochemical measurements for the films are conducted using back-side illumination (through the FTO-glass substrate to film). IPCE measurements were conducted using a full solar simulator (Newport, Model 9600, 150 W xenon lamp) with an AM 1.5 filter and a motorized monochromator (Oriel Cornerstone 130 1/8 m). The monochromator slit size was adjusted to 0.75 mm × 2 mm providing monochromatic wavelengths and a power density which could be adjusted from 12.8 and 252.3 μW/cm^2 of irradiation for wavelengths between 340 and 520 nm. A typical light power density used for the IPCE measurements can be found in Fig. S8. Light power was measured using a handheld optical power meter with a UV enhanced silicon photo-detector (Newport, Models 1916C and 818-UV). The IPCE is expressed by following equation:

$$\text{IPCE} = (1240 \times I)/(\lambda \times P_{light}) \quad (2)$$

where I is the measured photocurrent density at a specific wavelength (mA cm^{-2}), λ is the wavelength of incident light (nm) and P_{light} is the measured light power density at that wavelength (mW cm^{-2}) .

The electrochemical impedance spectroscopy (EIS) was performed using a CH Instruments 660D in 0.2 M Na_2SO_4 solution and 0.1 M phosphate buffer solution (pH 6.6). The Nyquist plots were measured at 0.8 V (*vs.* Ag/AgCl) with an AC amplitude of 5 mV, frequency of 100 kHz-100 mHz under AM 1.5 G illumination (100 mW/cm^2). The measured spectra were

fitted by using the Zview software. For converting the potential *vs.* Ag/AgCl to RHE the following equation was used:

$$E_{RHE} = E_{Ag/AgCl} + 0.059\,pH + 0.197\,V \quad (3)$$

Mott-Schottky measurements were conducted using a CH Instruments 660D and the built in software was used to measure capacitance *vs.* applied potential at a fixed frequency. Mott-Schottky plots were created and fit to ideal semiconductor behavior:

$$1/C^2 = (2/e\varepsilon\varepsilon_0 N_d)[V_a - V_{fb} - kT/e] \quad (4)$$

here C is the space charge layer capacitance, ε is the dielectric constant of the material, ε_0 is the permittivity of vacuum, e is the elemental charge, N_d is the concentration of charge carriers, V_a is the applied potential, V_{fb} is the flat band potential, k is Boltzmann's constant, and T is temperature.

3. Results and Discussion

Generally, the photoelectrochemical activity of $BiVO_4$ is dependent on their morphology, while the $BiVO_4$ morphology is strongly dependent on the synthesis condition and method. To optimize the photoelectrochemical activity, $BiVO_4$ films with different morphologies were synthesized on FTO substrates using a drop-casting method. The synthesis conditions and the corresponding products are summarized in Table 1.

Table 1 *Summary of synthesis conditions versus the $BiVO_4$ products.*

Sample no.	Bi:V:PEG-600 (volume ratio)	Precursor solution drying time (min)	Relevant Figure Number
1a	2 : 2 : 0	55	Fig. 1a and Fig. S1a
1b	2 : 2 : 1	55	Fig. 1b, 1c, Fig. S1b and Fig. 2b
1d	2 : 2 : 2	55	Fig. 1d and Fig. S1c
2a	2 : 2 : 1	0	Fig. 2a
2c	2 : 2 : 1	110	Fig. 2c

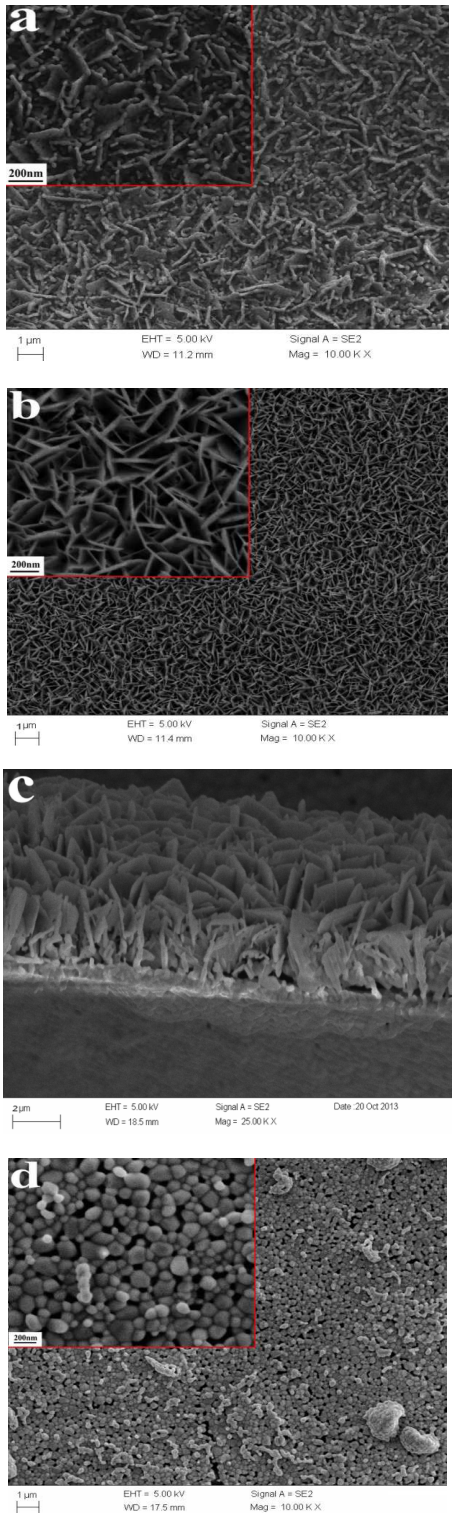

Fig. 1 *SEM images of $BiVO_4$ films on FTO substrate synthesized from a precursor solution containing Bi^{3+} , V^{3+} and PEG-600 with Bi: V: PEG-600 (volume ratio) = (a) 2:2:0, (b) and (c) 2:2:1, (d) 2:2:2.*

Fig. 1 shows SEM images for the $BiVO_4$ films synthesized from a precursor solution containing equal molar Bi^{3+} and V^{3+} with different amounts of polyethylene glycol 600 (PEG-600). As shown in Fig. 1a, non-uniform flake-like $BiVO_4$ are obtained from the PEG-600-free precursor solution. In addition, the edge of the film is cracked and the coverage is not uniform because of precursor solution bubbling during the annealing process (see Fig. S1a in the Supporting Information). Adding PEG-600 into the precursor solution (Bi: V: PEG-600=2:2:1, volume ratio) results in uniform $BiVO_4$ films on the FTO substrate (Fig. S1b). The top-view and cross-sectional images in Fig. 1b and 1c revealed that the $BiVO_4$ film is composed of flakes with an average thickness of 20 nm and length of 2 μm. Interestingly, the morphology of the $BiVO_4$ film completely changed when more PEG-600 was added into the precursor solution. As shown in Fig. 1d, the $BiVO_4$ film synthesized from a higher-concentration PEG-600 precursor solution (Bi: V: PEG-600=2:2:2) consists of agglomerated $BiVO_4$ nanoparticles. Additionally, the coverage, especially near the edge of the film is worse (see Fig. S1c), which is similar to $BiVO_4$ films synthesized from the PEG-600-free precursor solution. From these results, it is clear that the macroscopic homogeneity of the $BiVO_4$ film as well as the morphology is controllable by adding PEG-600 into the precursor solution. Polyethylene glycol (PEG) is commonly used as a morphology-directing agent for synthesizing nanostructured materials, usually acting by confining the crystal growth in certain directions.[33-35] It has been reported that PEG can play a role as the morphology-directing agent in synthesis of some metal oxides such as ZnO and Fe_3O_4 nanowires, mesoporous WO_3 and WO_3 nanoflakes.[30-32, 36] In the present work, to confirm the effect of PEG-600, we added polyethylene glycol 300 (PEG-300) into the precursor solution as a morphology-directing agent for synthesizing nanostructured $BiVO_4$, it was found that the $BiVO_4$ film synthesized from this precursor solution did not adhere well to the FTO substrate and the film consisted of highly non-uniform $BiVO_4$ (see Fig. S2, Supporting Information). The crystal structure of the films synthesized with varying PEG-600 content was determined by X-ray diffraction (XRD) and the patterns are shown in Fig. S3 of the Supporting Information. All of the as-synthesized films could be indexed to monoclinic $BiVO_4$ (JCPDS No. 01-075-1867).

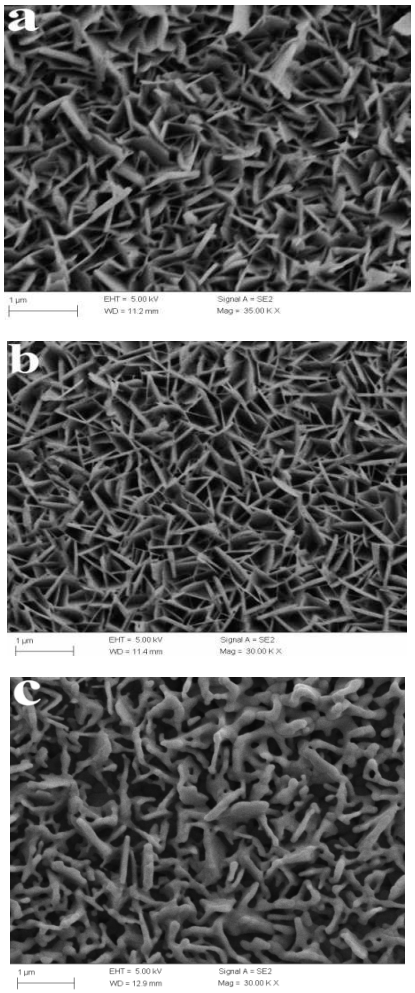

Fig. 2 *SEM images of $BiVO_4$ films on FTO substrate synthesized from a precursor solution containing Bi^{3+} , V^{3+} and PEG-600 (Bi: V: PEG-600=2:2:1) with (a) 0 min, (b) 55 min and (c) 110 min drying time for the precursor solution at 135 °C.*

The dependence of the $BiVO_4$ nanostructures on the precursor solution drying time is shown in Fig. 2. Fig. 2a shows a SEM image of the $BiVO_4$ film synthesized from the drop-casting method without a precursor solution drying process, i.e., the precursor solution was drop-cast on the FTO substrates, and then directly annealed at 500 °C for 2.5 hours. As shown in Fig. 2a, a flake array of $BiVO_4$ was formed, but the thickness of the flakes was not highly uniform. This may be attributed to the quick evaporation of precursor solution during the high temperature annealing process resulting in uneven growth of $BiVO_4$ crystals. We added an intermediate drying step for the precursor solution at 135 °C for 55 min to form a uniform colloid film and then annealed it at 500 °C for 2.5 hours. As shown in Fig. 2b, $BiVO_4$ nanoflake arrays were obtained after this drying step was included. Nevertheless, the colloidal $BiVO_4$ appears to agglomerate during a longer drying time (110 min), leading to larger, thicker $BiVO_4$ flakes (see Fig. 2c).

The photoelectrochemical activity of nanostructured $BiVO_4$ films (shown in Fig. 1a, Fig. 1b, Fig. 2a and Fig. 2c) was investigated by linear sweep voltammetry (LSV). The LSV measurements were conducted in 0.2 M Na_2SO_4 and 0.1M phosphate buffer solution (pH 6.6) illuminated with 100 mW/cm^2 simulated solar light. The LSV results indicated that the $BiVO_4$ film (shown in Fig. 1b and 2b) synthesized from the precursor solution with a Bi: V: PEG-600 volume ratio of 2:2:1 and dried at 135°C for 55 min has the best photoelectrochemical activity (see Fig. S4, Support Information). Thus, this precursor solution and drying condition was used to synthesize the un-doped and doped $BiVO_4$ films for subsequent experiments.

Based on previous studies, it was found that Mo and W doped $BiVO_4$ films have better photoelectrochemical activity than un-doped $BiVO_4$ films for water oxidation, especially 2.5% W doped, 5% Mo doped and 2% W, 6% Mo co-doped $BiVO_4$ films.[21,22] Herein we synthesized the corresponding doped $BiVO_4$ films by adding appropriate amounts of W and Mo into the $BiVO_4$ precursor solutions. As shown in Fig. 3, the doped $BiVO_4$ films exhibit similar morphology compared to the un-doped $BiVO_4$ films, although some small differences from the un-doped films due to the co-incorporation of W and Mo are visible. XRD performed on these films (Fig. 4) showed no tungsten or molybdenum oxide formation, implying the different morphology flakes are still single phase $BiVO_4$ flakes, but slight changes in crystal structure closer to tetragonal with Mo and/or W incorporation.

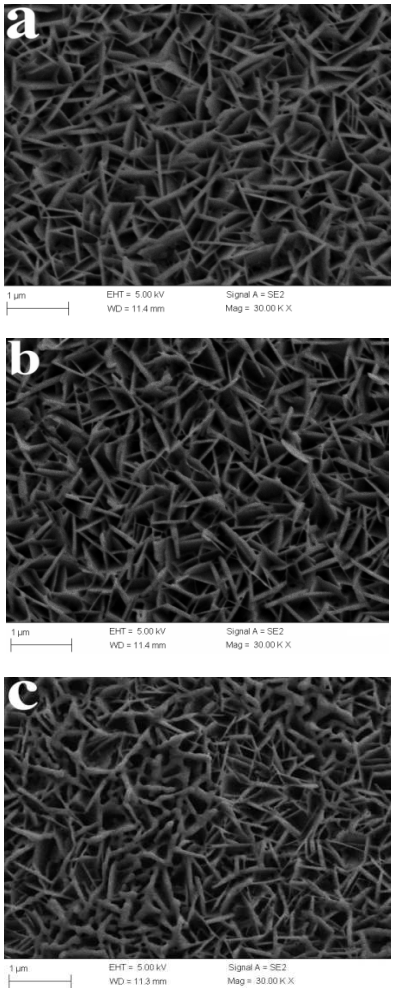

Fig. 3 *SEM images of (a) 2.5% W doped $BiVO_4$ film, (b) 5% Mo doped $BiVO_4$ film and (c) 2%W, 6% Mo co-doped $BiVO_4$ film.*

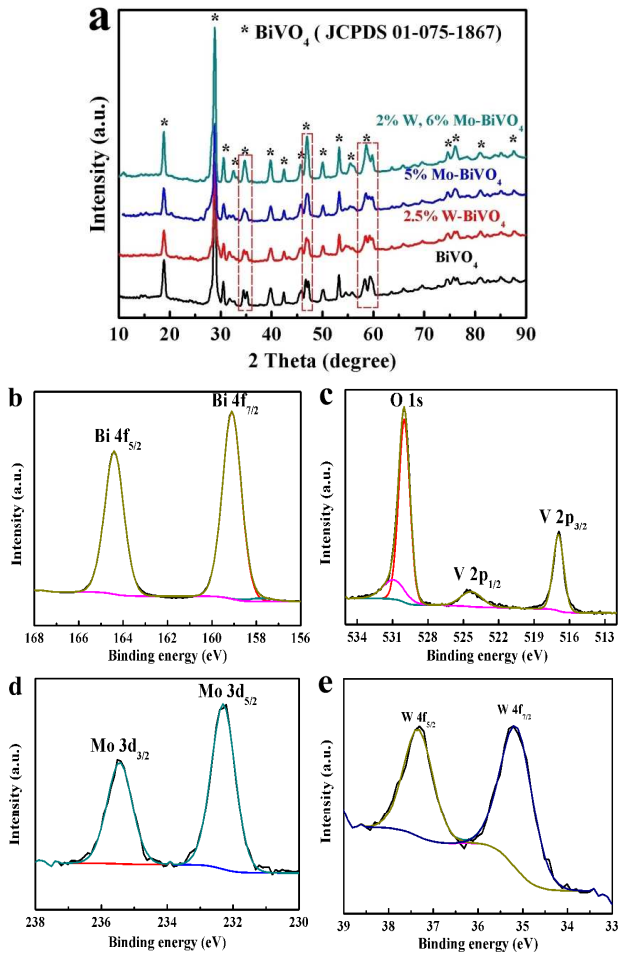

Fig.4 *(a) XRD patterns of $BiVO_4$, 2.5% W doped $BiVO_4$, 5% Mo doped $BiVO_4$, 2%W, 6% Mo co-doped $BiVO_4$. The boxes highlight the peaks that shift with W and Mo doping. High resolution XPS spectrum of (b) Bi 4f, (c) O 1s and V 2p, (d) Mo 3d and (e) W 4f.*

Table 2 *XPS data for $BiVO_4$ and doped $BiVO_4$ films*

Sample	XPS measured atomic ratio (Bi : V : W : Mo)	Designed atomic ratio (Bi : V : W : Mo)
$BiVO_4$	52 : 48 : 0 : 0	50 : 50 : 0 : 0
2.5% W-$BiVO_4$	49 : 48 : 3 : 0	48.75 : 48.75 : 2.5 : 0
5% Mo-$BiVO_4$	50 : 44 : 0 : 6	47.5: 47.5: 0: 5
2% W, 6%Mo-$BiVO_4$	51 : 42 : 2 : 5	46 : 46 : 2 : 6

The XRD measurements were conducted using powder samples that were scraped from the films. In the pure $BiVO_4$ pattern, all of the characteristic diffraction peaks are in good agreement with the standard data for monoclinic $BiVO_4$ (JCPDS No. 01-075-1867). For the doped samples, only peaks for monoclinic $BiVO_4$ were observed. However, as highlighted in Fig. 4a, three pairs of $BiVO_4$ peaks tended to merge into three single peaks after doping. For example, the (200) $BiVO_4$ peak at 34.5° and (002) peak at 35.2° shifted toward each other after 2.5% W doped into $BiVO_4$, and the two peaks merged into a single peak at 34.9° for 5% Mo doped and 2%W, 6% Mo co-doped $BiVO_4$ samples. This behavior was also observed for the (240) and (042) peaks at 46.7° and 47.9° and the (321) and (123) peaks at 58.3° and 59.4°. Similar observations were reported in previous work related to Mo and W doped $BiVO_4$.[21, 22] The merging of peaks can be attributed to a change in the crystal structure from monoclinic to tetragonal symmetry.[37] The surface composition of the films was verified by X-ray photoelectron spectroscopy (XPS) measurements. The high resolution XPS spectra of the Bi 4f, O 1s, V 2p, Mo 3d and W 4f binding energy regions for a representative 2%W, 6% Mo co-doped $BiVO_4$ sample are shown from Fig. 4b to 4e. The characteristic orbital splitting of the Bi $4f_{5/2}$ and Bi $4f_{7/2}$ peaks (Fig. 4b), and the V $2p_{1/2}$ and V $2p_{3/2}$ peaks (Fig. 4c) were observed with peak locations of 164.4, 159.1, 524.4 and 516.9 eV, respectively, closely matching the Bi^{3+} and V^{5+} peaks in monoclinic scheelite $BiVO_4$.[22, 38] For the O 1s peak, an additional small peak was seen which can be attributed to hydroxyls binding at defect sites.[22, 39] The Mo $3d_{3/2}$ and Mo $3d_{5/2}$ peaks were located at 235.4 and 232.2 eV (Fig. 4d), and the W 4f $_{5/2}$ and 4f $_{7/2}$ peaks were observed at 37.3 and 35.2 eV (Fig. 4e), confirming the presence of Mo^{6+} and W^{6+} species in $BiVO_4$.[40, 41] Using the XPS spectra, the Bi: V: W: Mo atomic ratios of the films were measured and are summarized in Table 2.

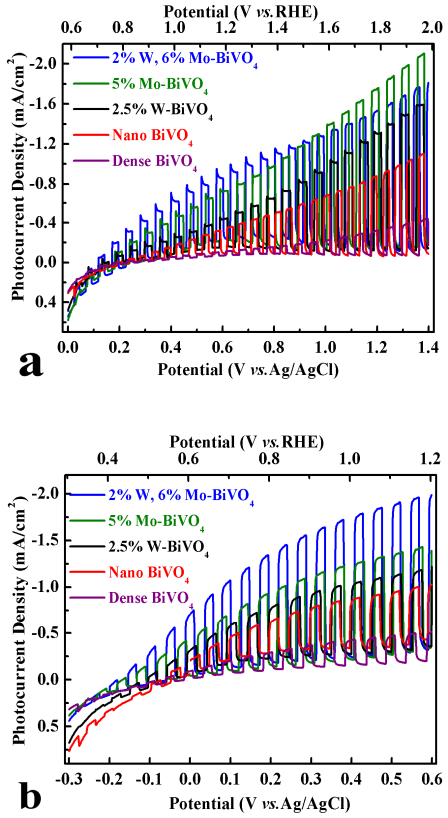

Fig.5 Average *chopped LSV scans for the $BiVO_4$ nanoparticle film, $BiVO_4$ nanoflake array film, 2.5% W doped $BiVO_4$ film, 5% Mo doped $BiVO_4$ film and 2% W, 6% Mo co-doped $BiVO_4$ film in (a) 0.2 M Na_2SO_4 and 0.1 M phosphate buffer solution (pH 6.6) and (b) 0.2 M Na_2SO_3 and 0.1 M phosphate buffer solution (pH 6.9) under illumination with 100 mW/cm^2 light. The scan rate was 25 mV/s.*

Fig. 5a shows the average chopped LSV collected from the $BiVO_4$ nanoparticle films (the film shown in Fig. 1d), $BiVO_4$ nanoflake array films (shown in Fig. 1b and 2b), 2.5% W doped $BiVO_4$ films (shown in Fig. 3a), 5% Mo doped $BiVO_4$ films (shown in Fig. 3b) and 2% W, 6% Mo co-doped $BiVO_4$ films (shown in Fig. 3c) in 0.2 M Na_2SO_4 and 0.1 M phosphate buffer solution (pH 6.6) illuminated with 100 mW/cm^2 light. The original LSV's measured on 12 films are shown in Fig. S5 of the supporting information. As shown in Fig. 5a, the lowest photocurrent was generated by the $BiVO_4$ nanoparticle film. In contrast, the $BiVO_4$ nanoflake array film showed a more pronounced photoresponse, indicating that the nanoflake structure is advantageous for achieving higher photoelectrochemical activity. For example, at 1.0 V *vs.* Ag/AgCl, the photocurrent density for the nanoflake array film was 0.68 mA/cm^2 and 0.23 mA/cm^2 for the nanoparticle film. The higher activity of the $BiVO_4$ nanoflake array film is due to a larger film/electrolyte interfacial area and reduction of the necessary holes transport length compared to the nanoparticle film. After doping with W and Mo, the nanostructured $BiVO_4$ films show further enhanced activity. With respect to the photocurrent density for the doped $BiVO_4$ films, there is little difference between the 5% Mo-$BiVO_4$ film (1.29 mA/cm^2 at 1.0 V *vs.* Ag/AgCl) and the 2% W, 6% Mo co-doped $BiVO_4$ film (1.28 mA/cm^2 at 1.0 V *vs.* Ag/AgCl), but both are higher than that for the 2.5% W-$BiVO_4$ film (0.91 mA/cm^2 at 1.0 V *vs.* Ag/AgCl). For further comparison, we tested the films in 0.1 M phosphate buffer (pH 6.9) with 0.2 M Na_2SO_3 added as a hole scavenger. In general, the results (see Fig. 5b) are consistent with the chopped LSV results measured in the buffered 0.2 M Na_2SO_4. Namely, the photoelectrochemical activity of the $BiVO_4$ nanoflake array film was better than that of the nanoparticle film and the doped $BiVO_4$ films' activity was higher than the un-doped $BiVO_4$ films. It is noteworthy that the 2% W, 6% Mo co-doped $BiVO_4$ film shows the highest photocurrent out of all the films tested in Na_2SO_3 solution. In summary, the photoelectrochemical activity of the films can be ranked in the following order: $BiVO_4$ nanoparticle film < $BiVO_4$ nanoflake array film < 2.5% W-$BiVO_4$ nanoflake array film < 5% Mo-$BiVO_4$ nanoflake array film < 2%W, 6% Mo-$BiVO_4$ nanoflake array film. The present results are similar to our previous study and a scanning electrochemical microscopy study of $BiVO_4$ doping that found W, Mo co-doped $BiVO_4$ resulted in higher

photoelectrochemical activity for water oxidation than individual Mo and W doped $BiVO_4$ and un-doped $BiVO_4$.[21, 22] DFT calculations suggest that W and Mo can act as effective shallow donors to increase the total carrier density, which could result in enhanced photoelectrochemical activity.[21, 23, 42] On the other hand, experimental data from Abdi *et al* showed that W doping of $BiVO_4$ decreases the carrier mobility by introducing mid-bandgap defects which act as carrier traps.[20] DFT calculations show that W and Mo doping into $BiVO_4$ may produce excellent *n*-type conductivity.[42] And Hoffart et al. showed that 5% Mo doped $BiVO_4$ had a total conductivity at least an order of magnitude higher than $BiVO_4$ at 600°C.[43] Thus, the improved conductivity in doped $BiVO_4$ may enhance its photoelectrochemical activity.

In order to understand the origin of the photoelectrochemical activity enhancement in the doped film, we investigated the optical behavior of the films using UV-vis absorbance spectroscopy (see Fig. S6a). Regardless of the amount of W and Mo incorporation, all of the films had a band gap of approximately 2.4 eV (Fig. S6b) and similar absorbed photon flux, indicating this cannot be the sole cause of the increased photoactivity (Fig. S6c). In addition, the water oxidation kinetics at the interface of the photoanode/electrolyte were evaluated by electrochemical impedance spectroscopy (EIS).[23, 28, 44] The EIS spectra are presented as Nyquist plots in Fig. 6a. The EIS measurements were performed in 0.2 M Na_2SO_4 and 0.1 M phosphate buffer solution (pH 6.6) under simulated solar light illumination (100 mW/cm^2). The Nyquist plots were interpreted in terms of the equivalent circuit shown in the inset of Fig. 6a. In the plot, the symbols indicate the experimental results and the lines represent fitting results. In the equivalent circuit, Rs is the solution resistance, CPE is the constant phase element for the electrolyte/electrode interface, and Rct is the charge transfer resistance across the electrode/electrolyte interface. The arcs in the Nyquist plot are related to charge transfer at the interface of the electrode/electrolyte. As shown in Fig. 6a, under illumination both Nyquist diagrams display a typical semicircle arc in the measured frequency region, and the semicircle arc for the 2% W, 6% Mo co-doped $BiVO_4$ film was smaller than that for the $BiVO_4$ film, indicating faster water oxidation kinetics. As shown in Table 3, the Rct value for the $BiVO_4$ film was 3216 Ω and for the 2% W, 6% Mo co-doped $BiVO_4$ film the value was 2931 Ω. Therefore, the enhanced photoelectrochemical activity for the 2% W, 6% Mo co-doped $BiVO_4$ film may be ascribed to the enhanced water oxidation kinetics.

The flat band potentials of the $BiVO_4$ nanoflake array film and the 2% W, 6% Mo co-doped $BiVO_4$ film were also measured in 0.2 M Na_2SO_4 and 0.1 M phosphate buffer solution (pH 6.6). Fig. 6b and 6c present the Mott–Schottky plots ($1/C^2$ *vs.* V) measured at different frequencies. The Mott–Schottky plots for the $BiVO_4$ and the co-doped BiVO4 film both showed quasi-linear behavior. The plots indicate that the flat band potentials of the $BiVO_4$ film and 2% W, 6% Mo co-doped $BiVO_4$ film were around -0.45 V and -0.35 V (*vs.* Ag/AgCl), respectively. Although the measured flat band potentials have certain deviations due to nanostructuring,[45] since the deviations should be similar for both films, it seems that that the flat band position of the co-doped $BiVO_4$ film shows a positive shift of about 100 mV compared with the un-doped $BiVO_4$ film. This is consistent with previous work related to W and Mo doped $BiVO_4$ showing a positive shift of the flat band potential.[21-23]

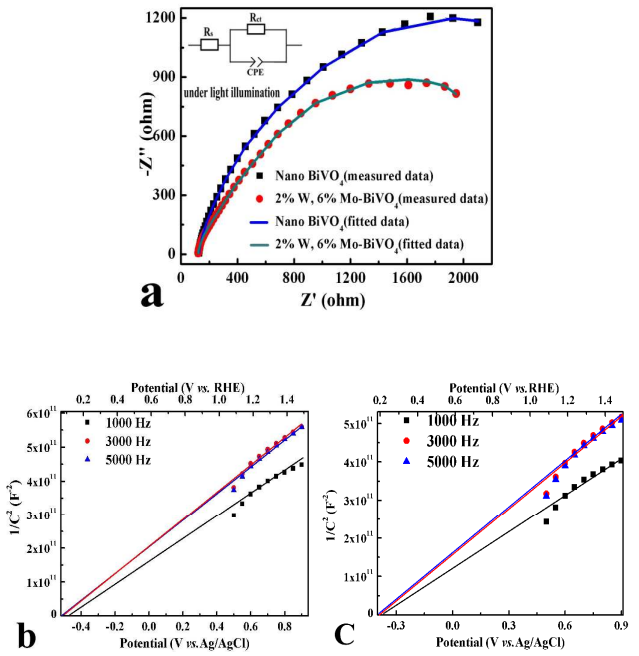

Fig. 6 *(a) Electrochemical impedance spectra of the $BiVO_4$ and 2% W, 6% Mo co-doped $BiVO_4$ film under simulated solar illumination (100 mW/cm^2). The solid line was fitted by Zview software using the proposed equivalent circuit model. The EIS was measured at 0.8 V (vs. Ag/AgCl) in 0.2 M Na_2SO_4 solution and 0.1 M phosphate buffer solution (pH 6.6). The inset shows an equivalent circuit for the photoanodes. Mott–Schottky plots for (b) the $BiVO_4$ nanoflake array film and (c) 2% W, 6% Mo co-doped $BiVO_4$ nanoflake array film. The measurements were conducted in 0.2 M Na_2SO_4 solution and 0.1 M phosphate buffer solution (pH 6.6).*

Table 3 *The values of the elements in equivalent circuit fitted in the Nyquist plots of Fig. 6a.*

Sample	Rs (Ω) /Error(%)	CPE1-T(F) / Error(%)	CPE1-P / Error(%)	Rct(Ω) / Error(%)
$BiVO_4$	116.2/1.16	9.56E-6/5.04	0.782/0.92	3216/3.23
2% W, 6% Mo-$BiVO_4$	114.4/1.25	2.61E-5/5.02	0.684/1.08	2931/3.84

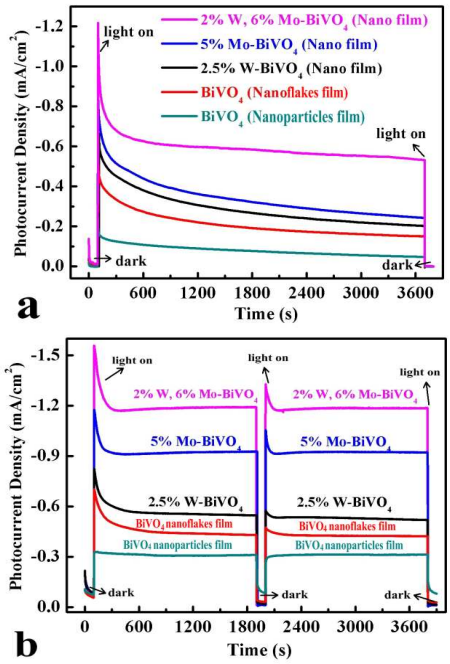

Fig. 7 *Amperometric i-t curve for the $BiVO_4$ nanoparticle film, $BiVO_4$ nanoflake array film, 2.5% W doped $BiVO_4$ film, 5% Mo doped $BiVO_4$ film and 2% W, 6% Mo co-doped $BiVO_4$ film under illumination with 100 mW/cm^2 light in (a) 0.2 M Na_2SO_4 and 0.1 M phosphate buffer solution (pH 6.6) at a constant applied potential of 1.0 V vs.Ag/AgCl (1.59 V vs RHE) and (b) 0.2 M Na_2SO_3 and 0.1 M phosphate buffer solution (pH 6.9) at a constant applied potential of 0.5 V vs.Ag/AgCl (1.1 V vs RHE).*

The stability of the films was investigated by chronoamperometry. We first conducted stability testing in 0.2 M Na_2SO_4 solution and 0.1 M phosphate buffer solution (pH 6.6) at a constant applied potential of 1.0 V *vs.* Ag/AgCl. As shown in Fig. 7a, the photocurrent on all of the films decreased after 3600 seconds of testing under illumination in Na_2SO_4 solution, which was mainly ascribed to material photocorrosion and vanadium dissolution.[15, 46] XPS analysis of the $BiVO_4$ film reveals that the atomic ratio of Bi/V decreased from 52/48 to 55/45 after the stability testing, indicating a loss of vanadium at the surface. Furthermore, the SEM images acquired from the $BiVO_4$ film shows that the $BiVO_4$ nanoflakes were damaged after 3600 seconds of illumination during stability testing (see Fig.S7 in

Supporting Information). However, the photoelectrochemical activity of the films tend to stabilize after the rapid initial decrease in photocurrent in 0.2 M Na_2SO_3 solution and 0.1 M phosphate buffer solution (pH 6.9) (see Fig. 7b) because of the protection provided by SO^{3-} against the photocorrosion. This indicates that the corrosion mainly occurs at the surface and the holes may be quickly injected into the SO^{3-} before having a chance to promote a reaction within the $BiVO_4$. Generally, the i-t testing results are consisitant with the chopped LSV results in Na_2SO_3 solution. On the other hand, the 2% W, 6% Mo co-doped $BiVO_4$ film showed the highest photocurrent retention both in Na_2SO_4 and Na_2SO_3 solution, this point is a little different from the chopped LSV result measured in Na_2SO_4 where 5% Mo doped films have the highest photocurrent.

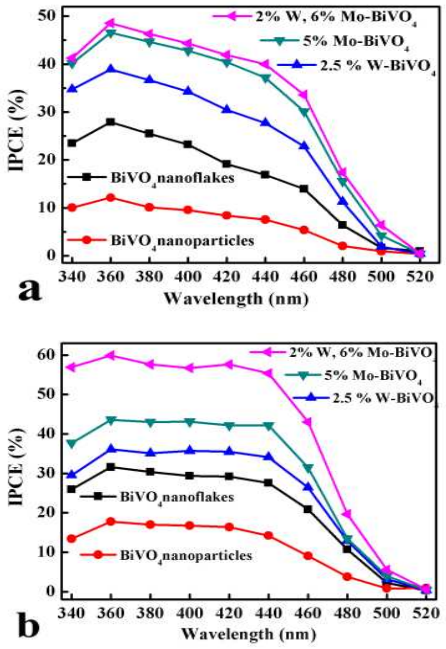

Fig. 8 *IPCE spectra for the $BiVO_4$ nanoparticle film, $BiVO_4$ nanoflake array film, 2.5% W doped $BiVO_4$ film, 5% Mo doped $BiVO_4$ film and 2% W, 6% Mo co-doped $BiVO_4$ film in (a) 0.2 M Na_2SO_4 and 0.1 M phosphate buffer solution (pH 6.6) at a constant applied potential of 1.0 V vs.Ag/AgCl (1.59 V vs RHE) and (b) 0.2 M Na_2SO_3 and 0.1 M phosphate buffer solution (pH 6.9) at a constant applied potential of 0.5 V vs.Ag/AgCl (1.1 V vs RHE).*

The relationship between the photoelectrochemical activity and the wavelength of the incident light was investigated by incident photon-to-current conversion efficiency (IPCE). Fig. 8 shows the IPCE spectra for the films measured in 0.2 M Na_2SO_4 buffered solution at 1.0 V *vs.*Ag/AgCl and 0.2 M Na_2SO_3 buffered solution at 0.5 V (*vs.*Ag/AgCl), the spectra are integrated and compared to the LSV results in Tables S1 and S2. For all of the films, the photoresponse was observed from 340 to 520 nm, which is in agreement with their UV-vis absorbance spectra. Additionally, in comparison to the $BiVO_4$ films, the doped $BiVO_4$ films exhibit enhanced IPCE over the entire absorption region and the 2% W, 6% Mo co-doped $BiVO_4$ film presents the highest IPCE. The IPCE results further confirmed W and Mo co-doping of $BiVO_4$ enhances the harvesting of photons for photoelectrochemical reactions.

4. Conclusions

In summary, a simple drop-casting method was developed to synthesize un-doped and doped $BiVO_4$ nanoflake array films on FTO coated glass substrates. The influence of synthesis parameters including the amount of polyethylene glycol 600 (PEG-600) and the precursor solution drying time on the growth of $BiVO_4$ film were investigated to optimize the films for photoelectrochemical water oxidation. The $BiVO_4$ films synthesized from a precursor solution containing Bi^{3+}, V^{3+} and PEG-600 with a Bi: V: PEG-600 volume ratio of 2: 2: 1 dried at 135°C for 55 min were composed of nanoflake arrays with an average thickness of 20 nm and length of 2 µm. The electrochemical results show that the $BiVO_4$ nanoflake array films have higher photoelectrochemical activity than the $BiVO_4$

nanoparticle films. Additionally, further enhanced photoelectrochemical activity was observed on the 2% W and 6% Mo co-doped $BiVO_4$ film. We believe that this facile drop-casting method may be suitable for synthesizing nanostructured $BiVO_4$-based materials for use in solar energy devices.

Notes

[a] *McKetta Department of Chemical Engineering and Department of Chemistry, University of Texas at Austin, 1 University Station C0400, Austin, Texas 78712-0231, United States Fax: (512) 471-7060; Tel: (512) 471-5817; E-mail: mullins@che.utexas.edu*

[b] *College of Chemistry and Chemical Engineering, Chongqing University, Chongqing 400030, China.*

[c] *College of Physics, Chongqing University, Chongqing 400030, China.*

† Electronic Supplementary Information (ESI) available: Photographs of $BiVO_4$ films, XRD patterns of $BiVO_4$, SEM images of $BiVO_4$, LSV scans for nanostructured $BiVO_4$ films, UV-vis absorbance spectra and Tauc plots of the films, the incident light power density spectrum used for the IPCE measurements and the integral photocurrent values for the films using the IPCE data. See DOI: 10.1039/b000000x/

Acknowledgements

The authors gratefully acknowledge the Division of Chemical Sciences, Geosciences, and Biosciences, Office of Basic Energy Sciences of the U.S. Department of Energy through Grant DE-FG02-09ER16119, and the Welch Foundation (Grant F-1436) for funding this work. Huichao He thanks the China Scholarship Council for financial support.

References

1. P. Yang, H. Yan, S. Mao, R. Russo, J. Johnson, R. Saykally, N. Morris, J. Pham, R. He and H. J. Choi, *Advanced Functional Materials*, 2002, **12**, 323-331.
2. X. Wen, S. Wang, Y. Ding, Z. L. Wang and S. Yang, *The Journal of Physical Chemistry B*, 2004, **109**, 215-220.
3. K. Zhu, N. R. Neale, A. Miedaner and A. J. Frank, *Nano Letters*, 2006, **7**, 69-74.
4. Y. Guo, X. Quan, N. Lu, H. Zhao and S. Chen, *Environmental Science & Technology*, 2007, **41**, 4422-4427.
5. J. Su, L. Guo, S. Yoriya and C. A. Grimes, *Crystal Growth & Design*, 2009, **10**, 856-861.
6. B. Liu and E. S. Aydil, *Journal of the American Chemical Society*, 2009, **131**, 3985-3990.
7. S. K. Mohapatra, S. E. John, S. Banerjee and M. Misra, *Chemistry of Materials*, 2009, **21**, 3048-3055.
8. G. Wang, D. Chen, H. Zhang, J. Z. Zhang and J. Li, *The Journal of Physical Chemistry C*, 2008, **112**, 8850-8855.
9. H. Zhang, X. Liu, Y. Li, Q. Sun, Y. Wang, B. J. Wood, P. Liu, D. Yang and H. Zhao, *Journal of Materials Chemistry*, 2012, **22**, 2465-2472.
10. K. Shankar, J. I. Basham, N. K. Allam, O. K. Varghese, G. K. Mor, X. Feng, M. Paulose, J. A. Seabold, K.-S. Choi and C. A. Grimes, *The Journal of Physical Chemistry C*, 2009, **113**, 6327-6359.
11. S. Shen, C. X. Kronawitter, J. Jiang, S. S. Mao and L. Guo, *Nano Research (2011-)*, 2012, **5**, 327-336.
12. C. Zhen, L. Wang, G. Liu, G. Q. Lu and H.-M. Cheng, *Chemical Communications*, 2013, **49**, 3019-3021.
13. S. Hoang, S. P. Berglund, N. T. Hahn, A. J. Bard and C. B. Mullins, *Journal of the American Chemical Society*, 2012, **134**, 3659-3662.
14. Q. Jia, K. Iwashina and A. Kudo, *Proceedings of the National Academy of Sciences*, 2012.
15. S. P. Berglund, D. W. Flaherty, N. T. Hahn, A. J. Bard and C. B. Mullins, *The Journal of Physical Chemistry C*, 2011, **115**, 3794-3802.
16. Z. Chen, T. F. Jaramillo, T. G. Deutsch, A. Kleiman-Shwarsctein, A. J. Forman, N. Gaillard, R. Garland, K. Takanabe, C. Heske, M. Sunkara, E. W. McFarland, K. Domen, E. L. Miller, J. A. Turner and H. N. Dinh, *Journal of Materials Research*, 2010, **25**, 3-16.
17. D. K. Zhong, S. Choi and D. R. Gamelin, *Journal of the American Chemical Society*, 2011, **133**, 18370-18377.
18. F. F. Abdi and R. van de Krol, *The Journal of Physical Chemistry C*, 2012, **116**, 9398-9404.
19. A. J. E. Rettie, H. C. Lee, L. G. Marshall, J.-F. Lin, C. Capan, J. Lindemuth, J. S. McCloy, J. Zhou, A. J. Bard and C. B. Mullins, *Journal of the American Chemical Society*, 2013, **135**, 11389-11396.
20. F. F. Abdi, T. J. Savenije, M. M. May, B. Dam and R. van de Krol, *The Journal of Physical Chemistry Letters*, 2013, **4**, 2752-2757.
21. H. S. Park, K. E. Kweon, H. Ye, E. Paek, G. S. Hwang and A. J. Bard, *The Journal of Physical Chemistry C*, 2011, **115**, 17870-17879.
22. S. P. Berglund, A. J. E. Rettie, S. Hoang and C. B. Mullins, *Physical Chemistry Chemical Physics*, 2012, **14**, 7065-7075.
23. K. P. Parmar, H. J. Kang, A. Bist, P. Dua, J. S. Jang and J. S. Lee, *ChemSusChem*, 2012, **5**, 1926-1934.

24. F. F. Abdi, N. Firet and R. van de Krol, *ChemCatChem*, 2013, **5**, 490-496.
25. G. Wang, Y. Ling, X. Lu, F. Qian, Y. Tong, J. Z. Zhang, V. Lordi, C. Rocha Leao and Y. Li, *The Journal of Physical Chemistry C*, 2013, **117**, 10957-10964.
26. J. A. Seabold and K.-S. Choi, *Journal of the American Chemical Society*, 2012, **134**, 2186-2192.
27. S. K. Pilli, T. E. Furtak, L. D. Brown, T. G. Deutsch, J. A. Turner and A. M. Herring, *Energy & Environmental Science*, 2011, **4**, 5028-5034.
28. S. J. Hong, S. Lee, J. S. Jang and J. S. Lee, *Energy & Environmental Science*, 2011, **4**, 1781-1787.
29. J. Su, L. Guo, N. Bao and C. A. Grimes, *Nano Letters*, 2011, **11**, 1928-1933.
30. Z. Li, Y. Xiong and Y. Xie, *Inorganic Chemistry*, 2003, **42**, 8105-8109.
31. J. K. Kim, K. Shin, S. M. Cho, T.-W. Lee and J. H. Park, *Energy & Environmental Science*, 2011, **4**, 1465-1470.
32. Q. Chen, J. Li, B. Zhou, M. Long, H. Chen, Y. Liu, W. Cai and W. Shangguan, *Electrochemistry Communications*, 2012, **20**, 153-156.
33. A. Wolcott, T. R. Kuykendall, W. Chen, S. Chen and J. Z. Zhang, *The Journal of Physical Chemistry B*, 2006, **110**, 25288-25296.
34. M. A. Tshabalala, B. F. Dejene and H. C. Swart, *Physica B: Condensed Matter*, 2012, **407**, 1668-1671.
35. G.-Y. Zhang, Y.-Y. Xu, D.-Z. Gao and Y.-Q. Sun, *Journal of Alloys and Compounds*, 2011, **509**, 885-890.
36. F. A. Harraz, *Physica E: Low-dimensional Systems and Nanostructures*, 2008, **40**, 3131-3136.
37. J. D. Bierlein and A. W. Sleight, *Solid state communications*, 1975, **16**, 69-70.
38. L. Zhang, D. Chen and X. Jiao, *The Journal of Physical Chemistry B*, 2006, **110**, 2668-2673.
39. H. Bluhm, *Journal of Electron Spectroscopy and Related Phenomena*, 2010, **177**, 71-84.
40. J. G. Choi and L. T. Thompson, *Applied Surface Science*, 1996, **93**, 143-149.
41. A. Katrib, F. Hemming, P. Wehrer, L. Hilaire and G. Maire, *Journal of Electron Spectroscopy and Related Phenomena*, 1995, **76**, 195-200.
42. W.-J. Yin, S.-H. Wei, M. M. Al-Jassim, J. Turner and Y. Yan, *Physical Review B*, 2011, **83**, 155102.
43. L. Hoffart, U. Heider, L. Jorissen, R. A. Huggins and W. Witschel, *Solid State Ionics*, 1994, **72**, 195-198.
44. K. Zhang, X.-J. Shi, J. K. Kim and J. H. Park, *Physical Chemistry Chemical Physics*, 2012, **14**, 11119-11124.
45. I. Cesar, K. Sivula, A. Kay, R. Zboril and M. Gra□tzel, *The Journal of Physical Chemistry C*, 2008, **113**, 772-782.
46. K. Sayama, A. Nomura, T. Arai, T. Sugita, R. Abe, M. Yanagida, T. Oi, Y. Iwasaki, Y. Abe and H. Sugihara, *The Journal of Physical Chemistry B*, 2006, **110**, 11352-11360.